arXiv:0810.3271v1 [cond-mat.mtrl-sci] 17 Oct 2008

Density matrix calculation of optical constants from optical to x-ray frequencies

M. P. Prange,[1] J. J. Rehr,[1] G. Rivas,[2] J. J. Kas,[1] and John W. Lawson[3]

[1]*Department of Physics, University of Washington, Seattle, WA 98195*

[2]*Instituto de Ingeniería y Tecnología,*

Universidad Autónoma de Ciudad Juárez, Juárez, 32310 Mexico

[3]*Mail Stop 229-1, NASA Ames Research Center, Moffett Field, California 94035*

(Dated: October 29, 2018)

Abstract

We present a theory of linear optical constants based on a single-particle density matrix and implemented in an extension of the real-space multiple scattering code FEFF. This approach avoids the need to compute wave-functions explicitly, and yields efficient calculations for frequencies ranging from the IR to hard x-rays, and applicable to arbitrary aperiodic systems. Our approach is illustrated with calculations of optical properties and applications for several materials.

I. INTRODUCTION

This work is primarily concerned with theoretical calculations of *optical constants*, which are obtained from the long-wavelength limit $\vec{q} \to 0$ of the dielectric function $\epsilon(\vec{q}, \omega)$. These include the complex dielectric constant $\epsilon(\omega)$, the complex index of refraction, the energy-loss function, the photoabsorption coefficient, the photon scattering amplitude per atom, and the optical reflectivity. The *ab initio* calculation of these optical properties for arbitrary materials has been a long-standing problem in condensed-matter physics.[1,2,3,4,5] Thus in practice, these properties are often estimated from atomic calculations or taken from tabulated sources.[6,7,8,9] However, such tabulations are available only for a small number of materials over limited spectral ranges. Thus we aim to develop an efficient and widely applicable method covering a broad range of frequencies, thereby providing a practical alternative or complement to tabulated data.

The theory of dielectric response of crystalline systems has been developed extensively over the past several decades,[1] following pioneering works of Nozières and Pines,[2] Ehrenreich and Cohen,[3] Adler,[4] and Wiser.[5] These works developed the self-consistent field approach for the dielectric function within the time-dependent Hartree approximation, also known as the random phase approximation (RPA). Subsequently the theory has been extended to include exchange effects within the time-dependent density functional theory (TDDFT).[10,11] While ground-state DFT calculations are now routine, theoretical methods for accurate calculations of optical spectra are still not widely available. More elaborate theories have been developed that take into account quasi-particle effects and particle-hole interactions based on the Bethe-Salpeter equation (BSE),[12,13,14] but these are even more computationally demanding.

In order to remedy this situation we have developed an efficient, real-space approach within the adiabatic local-density approximation that can be applied to arbitrary condensed systems over a broad range of frequencies from the visible to hard x-rays. Our approach is based on a density matrix formulation within an effective single-particle theory. This approach is a generalization of the real-space Green's function method implemented in the FEFF codes that includes both core- and valence-level spectra. Our work is intended to extend the capabilities and ease-of-use of FEFF to enable *full spectrum* output for general aperiodic systems with a quality roughly comparable to that in currently available tabulated

data.[6,7,8,9] This effort was begun by one of us using an atomic approximation for initial states.[15] This approximation is often adequate at high frequencies, but is unsatisfactory for optical and UV spectra.

The remainder of this paper is arranged as follows. Sec. II. describes the theoretical formalism behind our approach; Sec. III. presents typical results for various optical constants for a number of materials; Sec. IV. discusses some additional applications and diagnostics, and Sec. V. presents a brief summary and conclusions.

II. THEORY

A. Density matrix theory of dielectric response

We consider the macroscopic linear response of extended systems to an external electromagnetic field of polarization $\hat{\epsilon}$ and frequency ω

$$V_{\rm ext}(t) = V_{\rm ext}(\omega)e^{(-i\omega+\delta)t} + cc, \tag{1}$$

where δ is a positive infinitesimal corresponding to adiabatic turn-on of the perturbing potential. Throughout this work we use Hartree atomic units ($\hbar = m = e^2 = a_0 = 1$) unless otherwise specified. This perturbation polarizes the material, inducing a steady-state change $\delta n(\vec{r},\omega)e^{-i\omega t} + cc$ in the microscopic electron density, which leads to a macroscopic polarization $\vec{P}(\omega)e^{-i\omega t} + cc$, representing the average *screening* dipole response of the electrons to the applied field. For simplicity of discussion, we assume that $\vec{P}$ has no component perpendicular to the applied electric field. This is the case for systems of cubic or higher symmetry in the $q \to 0$ limit, but relaxing this restriction poses no computational difficulty. In this case one can define a scaler electric susceptibility χ, and the dielectric function is [16]

$$\begin{aligned} \epsilon(\omega) &= 1 + 4\pi\chi(\omega) \\ \vec{P} &= \chi\vec{E}, \end{aligned} \tag{2}$$

where $\vec{E}$ is the electric field. Our calculations here make use of an effective single-particle microscopic theory in which the N-electron state of the system at time t is described by a Slater determinant of time-dependent single-particle orbitals $\phi_i(t)$. Thus the state can be characterized by the single-particle density matrix ρ which is simply the projector onto the

orbitals:

$$\rho(t) = \sum_{i=1}^{N} |\phi_i(t)\rangle \langle\phi_i(t)| . \tag{3}$$

Their time evolution is governed by the time-dependent Schrodinger equation

$$i\frac{d}{dt}|\phi_i(t)\rangle = H|\phi_i(t)\rangle \tag{4}$$

for the time-dependent Kohn-Sham Hamiltonian

$$H = -\frac{1}{2}\nabla^2 + V_{\rm nuc} + V_H + V_{\rm xc} + \Sigma_d + V_{\rm ext}(t). \tag{5}$$

The terms in Eq. (5) are respectively the kinetic energy, the electrostatic attraction to the nuclei $V_{\rm nuc}$, the Hartree potential V_H, the ground-state exchange-correlation potential $V_{\rm xc}$, the dynamical contribution to the quasi-particle self-energy correction in the GW plasmon-pole approximation Σ_d, and the time-dependent external potential $V_{\rm ext}(t)$ of Equation (1). Here and below, we suppress the position dependence of quantities when no confusion will result. The time evolution in Eq. (4) implies the Liouville equation[3] for the density matrix

$$i\frac{d\rho}{dt} = H\rho - \rho H^\dagger. \tag{6}$$

In order to obtain the optical constants, we first linearize this equation with respect to the ground-state by decomposing the Hamiltonian and density matrix into their values in the ground-state and parts induced by $V_{\rm ext}$

$$\begin{aligned} H &= H_0 + H_1(t) = H_0 + V_{\rm ext}(t) + V_{\rm ind}(t) \\ \rho &= \rho_0 + \rho_1. \end{aligned} \tag{7}$$

H_1 consists of the external field and a term $V_{\rm ind}$ due to the response of the electrons. Second order terms, i.e., the products $\rho_1 H_1$ and $H_1\rho_1$ are discarded. We assume that the induced potential $V_{\rm ind}$ and hence H_1 *have the same time dependence as* $V_{\rm ext}$. With these assumptions, the time derivative in Eq. (6) becomes trivial and we can solve Eq. (6) for the induced density matrix in terms of the Kohn-Sham (KS) orbitals $|\phi_i^0\rangle$ and eigenvalues E_i of the ground-state system,

$$\rho_1(\omega) = \sum_{i,j}(f_i - f_j)\frac{|\phi_i^0\rangle \langle\phi_i^0|H_1|\phi_j^0\rangle \langle\phi_j^0|}{\omega - (E_j - E_i) + i\delta}, \tag{8}$$

where $f_i = f(E_i) \approx \theta(\mu - E_i)$ is the Fermi occupation number of state $|\phi_i^0\rangle$ and μ is the Fermi level. The KS orbitals obey the unperturbed Schrodinger equation

$$i\frac{d}{dt}|\phi_i(t)\rangle = H_0|\phi_i(t)\rangle . \tag{9}$$

The induced electron density $\delta n(\vec{r},\omega)$ due to the perturbation $V_{\rm ext}$ is then given by

$$\delta n(\vec{r},\omega) = \langle \vec{r} | \rho_1(\omega) | \vec{r} \rangle \, . \tag{10}$$

At this point it is convenient to introduce the bare and full susceptibilities whose local behavior is given by

$$\delta n(\vec{r},\omega) = \left\langle \vec{r} \middle| \chi^0(\omega) H_1 \middle| \vec{r} \right\rangle = \langle \vec{r} | \chi(\omega) V_{\rm ext} | \vec{r} \rangle \, . \tag{11}$$

Typically, the bare response χ^0 to an external perturbation is first computed from a single-particle (i.e. non-interacting) description of the ground state. The full response χ of the system can be related to response χ^0 of some non-interacting reference system. This procedure gives rise to the Dyson equation for χ with an interaction kernel K

$$\chi = \chi^0 + \chi^0 K \chi = \chi^0 (1 - K\chi^0)^{-1}. \tag{12}$$

Methods for computing optical response that start from a single-particle description of the ground state can be classified by their approximations to the particle-hole interaction kernel K. The accuracy of the calculated macroscopic properties reflect that of the non-interacting response and the interaction kernel. Note, in particular, that one needs to find the frequency-dependent response of the non-interacting system, which involves different considerations than those for static, ground state properties (e.g., the ground state energy and density).

In the crudest approximation $K = 0$: the resulting polarizability is that of the non-interacting reference system and local fields are neglected. In this case there is no screening, and the single-particle potential is the sum of the ground-state potential and $V^{\rm ext}$. An obvious deficiency of the non-interacting response is that the Coulomb field of the induced density is neglected. To address this deficiency Adler[4] and Wiser[5] developed formally equivalent theories of the macroscopic dielectric response of periodic solids based on the RPA in which K is taken to be the bare Coulomb interaction. These theories were originally built on band structure calculations for periodic materials in the Hartree approximation, and Hartree local fields were included through the now termed *Adler-Wiser formula*. In this approach the operator inversion of Eq. (12) is reformulated using the inverse of the microscopic dielectric matrix $\epsilon_{GG'}(\omega,\vec{k})$, which is then spatially averaged to give the macroscopic response $\epsilon(\omega) = \lim_{k\to 0} 1/[\epsilon^{-1}(\vec{k},\omega)]_{0,0}$. However, the Adler-Wiser dielectric function is that of the Hartree system and has the deficiency that the underlying electronic wave function is not anti-symmetric under particle interchange.

Going beyond RPA thus requires additional exchange-correlation effects in K. There have been efforts along these lines of two types: those based on time-dependent formulations of density-functional theory (TDDFT), and those based on many body perturbation theory and the BSE. These approaches have been critically compared by Onida et al.[1] By considering excited states from a quasi-particle viewpoint,[14] the interaction kernel can be decomposed into a direct term K^D which is the Coulomb interaction between the quasi-particles and an exchange interaction K^X,

$$K = K^X + K^D. \tag{13}$$

Expanding Eq. (12) in singly-excited (one electron, one hole) states and taking K^D to be the Coulomb interaction screened by an effective (microscopic) dielectric function, yields a set of approximations referred to as the Bethe-Salpeter Equation (BSE). Various screening models are used ranging from parametrized models (e.g. the Levine-Louie dielectric function) to independent-particle approximations such as the static RPA. BSE schemes can become computationally demanding since the inverse in Eq. (12) must be dealt with in a product basis which can be large. The differences between the independent-particle excitation energies and optical spectra and their interacting counterparts are referred to as excitonic effects. However, the non-locality of the exchange-correlation terms can be avoided by including exchange-correlation effects in K in terms of a density-functional $f_{\rm xc}$. Then the approach reduces to the TDDFT [10] where

$$K(\omega) = v + f_{\rm xc}(\omega), \quad f_{\rm xc}(\omega) = \frac{\delta V_{\rm xc}}{\delta \rho}. \tag{14}$$

Consequently a local approximation to $v_{\rm xc}$ leads to a local kernel (i.e., K depends only on the diagonal elements of the real-space single-particle density matrix). This locality implies that Eq. (12) can be expanded in a single-particle basis, thus circumventing the need for particle-hole states needed for the BSE. The cost of this simplification is that direct information about the particle-hole interaction (e.g. exciton wave-functions) is only implicit. This makes it difficult to systematically improve on the local density approximation (LDA)[1]. Nevertheless, calculations in such TDLDA frameworks have been carried out for a variety of systems.[17,18] While the TDDFT has achieved good agreement with experiment for optical spectra in many cases, quantitative agreement at higher frequencies has been more elusive. Calculations with the BSE tend to be even more computationally limited. In addition these methods are built on various ground-state KS calculations, depending on the system. Each

approach can work well for a specific class of materials, but can lose accuracy or applicability for others. Also, the ground-state methods used were originally developed to calculate static properties and calculations of frequency-dependent (non-interacting) response can become cumbersome due to the need for large basis sets and special exchange-correlation functionals to describe unoccupied and excited states.

The above difficulties have led us to consider a different approach with the goal of developing a general method for calculations of optical response that can handle a variety of systems and spectral ranges. Our approach is based on an extension of real-space multiple scattering theory (RSMS) in terms of the one-particle density matrix. The RSMS approach is well suited to treat arbitrary aperiodic condensed-matter systems over a very broad frequency range (from the visible to hard x-rays). Indeed, this scattering-theoretic approach provides a superior basis for very high energy spectra where scattering is weak and the approach converges rapidly. Further the approach goes beyond the Born-Oppenheimer approximation and can include nuclear motion effects in terms of correlated Debye-Waller factors.[19]

In this work, we present calculations within this RSMS approach using an independent quasi-particle approximation for the single particle states. Comparing Eq. (10) and (11) gives an expression for the bare response function or susceptibility

$$\chi^0(\vec{r},\vec{r}\,',\omega) = \sum_{i,j}(f_i - f_j)\frac{\phi_i^0(\vec{r})\phi_i^{0*}(\vec{r}\,')\phi_j^0(\vec{r}\,')\phi_j^{0*}(\vec{r})}{\omega - (E_j - E_i) + i\delta}. \tag{15}$$

Formally the imaginary part of the dielectric function is related to the full susceptibility by[10]

$$\epsilon_2(\omega) = \frac{4\pi}{V}\mathrm{Im}\int d\vec{r}\,d\vec{r}\,'\ \mathrm{Tr}\ d\,\chi(\vec{r},\vec{r}\,',\omega)\,d^\dagger, \tag{16}$$

where V is the volume of the system, and $d = \vec{\alpha}\cdot\epsilon_p e^{i\vec{k}\vec{r}}$ is the transition operator between the incident photon of wave vector $\vec{k}$ and polarization ϵ_p. In practice the transition operator is replaced by the truncation to rank-one of its expansion into tensors developed by Grant,[20] which is equivalent to the dipole approximation.

To evaluate Eq. (16) for both optical and x-ray frequencies, we must first compute the response function $\chi^0(\vec{r},\vec{r}\,',\omega)$. Formally Eq. (15) can be expressed in terms of the single-particle Green's function as

$$\begin{aligned}\chi^0(\vec{r},\vec{r}\,',\omega) = \int^{E_F} & \rho(\vec{r},\vec{r}\,',E)G^+(\vec{r},\vec{r}\,',E+\omega) \\ + & \ \rho(\vec{r}\,',\vec{r},E)G^-(\vec{r}\,',\vec{r},E-\omega)\,dE.\end{aligned} \tag{17}$$

Using the symmetries $\rho(\vec{r},\vec{r}',E)=\rho(\vec{r}',\vec{r},E)$ and $G^-(\vec{r},\vec{r}',E)=[G^+(\vec{r}',\vec{r},E)]^*$ on the real E-axis we can express the results entirely in terms of the one-particle density matrices $\rho(E)$

$$-\frac{\mathrm{Im}\,\chi^0}{\pi}=\int_{E_F-\omega}^{E_F}\rho(\vec{r}',\vec{r},E)\rho(\vec{r}',\vec{r},E+\omega)\,dE. \tag{18}$$

In this work we calculate these density matrices for energies ranging from the lowest occupied states to very high energies of order 100 KeV.[21]

B. Multiple scattering Green's function

Our calculations use an independent electron model in which each electron moves in an effective quasi-particle scattering potential $V(\vec{r})$ which implicitly includes a dynamic self-energy correction $\Sigma_d(E)$ to the ground state exchange and correlation potential. In this work $\Sigma_d(E)$ is calculated using the local GW plasmon-pole model of Hedin and Lundqvist.[22] The potential $V(\vec{r})=\sum_n v_n(r_n)+V_0$ is taken to be the self-consistent muffin-tin potential for a cluster of atoms at fixed locations $\vec{R}_n$. Here $\vec{r}_n=\vec{r}-\vec{R}_n$ is the position relative to the n^{th} atom, and V_0 is a constant interstitial potential. Within RSMS theory, the Green's function for this potential can be written as a double angular momentum expansion

$$\begin{aligned} G(\vec{r},\vec{r}',E) \;&=\; -2k\Big[\sum_{LL'}R_{Ln}(\vec{r}_n)\tilde{G}_{Ln,L'n'}\bar{R}_{L'n'}(\vec{r}'_{n'}) \\ &+\quad \delta_{n,n'}\sum_{L}H_{Ln}(\vec{r}_>)\bar{R}_{Ln'}(\vec{r}_<)\Big], \end{aligned} \tag{19}$$

where n and n' are the sites nearest $\vec{r}$ and $\vec{r}'$ respectively, and $\vec{r}_>$ ($\vec{r}_<$) is the larger (smaller) of the two position vectors. The terms in equation (19) are the right-hand-side regular and irregular solutions R_{Ln}, H_{Ln} of the spherically symmetric single-site problems and their left-side counterparts $\bar{R}_{Ln}$, $\bar{H}_{Ln}$, the partial-wave phase shifts δ_{ln}, and the multiple scattering (MS) matrix $G_{Ln,L'n'}$. The wave functions are normalized so that in the interstitial region R_{Ln} coincides with $Y_L[h_l^+e^{i\delta_{ln}}-h_l^-e^{-i\delta_{ln}}]/2i$, and H_{Ln} coincides with $Y_Lh_l^+e^{i\delta_{ln}}$. The bar for the left-sided solutions indicates that all factors except the Bessel functions are to be complex conjugated. Eq. (19) is rederived in the Appendix. As detailed in the Appendix, all these ingredients except the MS matrix can be found from the solution of a spherically symmetric single-particle quantum mechanics problem. The full MS matrix G for the system is found by numerical matrix inversion (e.g., with the LU or Lanczos algorithms in FEFF) with typical matrix dimensions of order 2×10^3 or using the MS path expansion.

C. Relativistic basis

To include relativistic effects such as spin-orbit coupling in our calculations properly it is necessary to recast the Green's function in terms of spinor solutions to the Dirac equation. In this context it is convenient to expand the spin-angular dependence of the one-electron states in the Pauli spinor-valued spin-orbit eigenfunctions which diagonalize both total and orbital angular momentum

$$\chi_K(\hat{r}) = \sum_{\sigma=-\frac{1}{2}}^{\frac{1}{2}} Y_l^{m_j-\sigma}(\hat{r})\phi^\sigma \left\langle l, \frac{1}{2}, m_j - \sigma, \sigma | j, m_j \right\rangle . \tag{20}$$

Here ϕ^σ is a Pauli spinor, $K = (\kappa, m_j)$ is a pair of relativistic angular momentum quantum numbers, and $\langle l, s, m_l, m_s | j, m_j \rangle$ is a Clebsh-Gordan coefficient. In this work as in Ref. [23] and [24], we have constructed the scattering matrix $G_{Ln,L'n'}$ of Eq. (19) using the scattering matrices t_l calculated for the total angular momentum channel $j = l + 1/2$. This matrix is then transformed to the basis of spin-orbit eigenfunctions using Clebsch-Gordan coefficients. The central-site contribution Eq. (A.17) is constructed directly from numerical solutions of the central-site problem giving a total relativistic Green's function

$$\begin{aligned} G(\vec{r}, \vec{r}', E) \;=\; & -2k\Big[\sum_{KK'} H_{Kn}(\vec{r}_>)\bar{R}_{K'n'}(\vec{r}_<)\delta_{KK'}\delta_{nn'} \\ & +\; R_{Kn}(\vec{r}_n)\tilde{G}_{KnK'n'}\bar{R}_{K'n'}(\vec{r}'_n)\Big], \end{aligned} \tag{21}$$

written in terms of right-hand (no bars) and left-hand (bars) solutions of the Dirac equation at energy E. These functions are 4-spinors which can be written in terms of the spin-orbit eigenfunctions:

$$\begin{aligned} R_{Kn}(\vec{r}_n) &= \frac{1}{r_n} \begin{pmatrix} P_\kappa(r_n)\chi_\kappa^{m_j}(\hat{r}_n) \\ iQ_\kappa(r_n)\chi_{-\kappa}^{m_j}(\hat{r}_n) \end{pmatrix} \\ \bar{R}_{Kn}(\vec{r}_n) &= \frac{1}{r_n} \begin{pmatrix} P_\kappa(r_n)\chi_\kappa^{m_j\dagger}(\hat{r}_n) \\ -iQ_\kappa(r_n)\chi_{-\kappa}^{m_j\dagger}(\hat{r}_n) \end{pmatrix}^{\mathrm{T}}, \end{aligned} \tag{22}$$

where the T in Eq. (22) denotes the transposed vector. The irregular solutions H, $\bar{H}$ take a similar form. These solutions are normalized by requiring the upper-component radial wave functions to coincide with $[h_l^+ e^{i\delta_{\kappa n}} - h_l^- e^{-i\delta_{\kappa n}}]/2i$ (regular solution) or $h_l^+ e^{i\delta_{\kappa n}}$ (irregular solution). We are using the notation of Grant,[20] where the reader is referred for details

regarding the numerical solutions P, Q appearing in Eq. (22). Tamura[25] gives a relevant and illuminating discussion of solutions to the Dirac equation in spherical coordinates, although he treats a more general case using different notation. We have also transformed to a basis of real spherical harmonics to simplify calculations of the real-valued density matrices.

D. Complex scattering potential

The construction of the self-consistent muffin-tin scattering potential for the one-particle states is described elsewhere,[26] and we only briefly summarize the process here. First, a Dirac-Fock solver is used to calculate free-atomic potentials and densities which are then overlapped to obtain a starting point for the self-consistency loop. In this loop the one-particle Green's function for the full multiple scattering problem is calculated, from which a new electron density is calculated. Finally a new ground state muffin-tin potential is constructed within the LDA. The loop is iterated to self-consistency which typically takes about 10-20 iterations. Self-energy corrections are subsequently added for unoccupied states within the GW plasmon-pole approximation.

E. Core state response

At low energies (below the bottom of the valence band), the density matrix becomes sparse in energy, taking non-zero values only at isolated eigenvalues. In this regime, it is more computationally efficient to use orbitals to describe the electronic structure. Thus, we separate the single particle density matrix into two energy regions: the core region in which the atomic approximation is valid and the solid-state region where solid-state corrections are important,

$$\rho(E) = \begin{cases} \rho^{\text{core}}(E) & E < E_{\text{cv}}, \\ \rho^{\text{val}}(E) & E > E_{\text{cv}}. \end{cases} \tag{23}$$

The core-valence separation energy E_{cv} is chosen to be an energy away from all KS eigenvalues that separates the two regimes and is set by default to -40 eV, which is typically about 30 eV below the Fermi level. Above this energy $\rho(E)$ is derived from the single-particle Green's function as described below. Note that in general there are occupied and unoccupied states above E_{cv}, but there are no unoccupied states below E_{cv}. Similarly, the

dielectric function $\epsilon_2(\omega)$can be separated into contributions $\epsilon_2^{\rm core}(\omega)$ and $\epsilon_2^{\rm val}(\omega)$ arising from transitions with core and valence initial states respectively.

The core states are represented by single-particle atomic-like orbitals ϕ_ν. Here the index $\nu = (n, i)$ denotes both a site index n and atomic level index i for the particular bound state at that site (e.g. 1s, 2s, $2p_{1/2}$, etc.). We replace $\rho(E)$ in Eq. (18) for $E < E_{\rm cv}$ with

$$\rho_{\rm core}(E) = \sum_\nu \rho_{\rm at}^{(\nu)}(E), \tag{24}$$
$$\rho_{\rm at}^{(\nu)}(E) = \phi_\nu(\vec{r})\phi_\nu(\vec{r}\,')\delta(E - \epsilon_\nu).$$

Thus we recover an expression equivalent to Fermi's golden rule for the absorption of light

$$\epsilon_2^{\rm core}(\omega) = \sum_\nu \epsilon_2^\nu(\omega) \tag{25}$$
$$= \frac{4\pi}{\omega} \sum_\nu {\rm Im}\langle\, i \,|\, \hat{d}^\dagger \hat{G}(\omega + \epsilon_i)\hat{d} \,|\, i \,\rangle \theta(\omega + \epsilon_i - \epsilon_F).$$

The initial core states $|\phi_\nu\rangle$ and their associated eigenvalues ϵ_ν are described accurately by Dirac-Fock atomic states for a single atomic configuration[27]. For energies below $E_{\rm cv} \approx \mu - 30$ Ev $< V_0$ the eigenfunctions of the central site problem are tightly bound to the central atom; their wave-functions decay rapidly as a function of the distance from the central site and can be taken to vanish in all cells except the central cell. This, along with the selection rules, limits the elements $G_{KnK'n'}$ (representing the final states) that contribute to absorption. For core initial states, the final state energy includes the inverse core-hole lifetime Γ_ν which broadens ϵ^ν. The calculation of the density matrix elements appearing in equation (16) is handled differently depending on the photoelectron energy $E = \omega + \epsilon_\nu$. For low-energy (less than $\approx$ 50 eV+V_0) final states G is calculated by FMS just as in the calculation of $\epsilon_2^{\rm val}$. At very high energies we again employ an atomic model and neglect scattering contributions (i.e. $G_{KnK'n'} = 0$ in Eq. (21)). At intermediate energies (50 eV $+V_0 \le E \le$ 1000 eV) we use efficient path filters[28] developed to treat EXAFS to find the dominant terms in the multiple scattering path expansion and sum these contributions to obtain the necessary $G_{KnK'n'}$ elements,

$$G = G^0 + G^0 T G^0 + \cdots . \tag{26}$$

The calculation of $\epsilon_2^{\rm core}$ is accomplished by looping over the edges ν with eigenvalues below $E_{\rm cv}$. For each edge we calculate ϵ_2^ν via FMS, path-expansion, and the atomic approximation

on appropriate energy grids. At this stage, correlated Debye-Waller factors can be included as in conventional XAS calculations using FEFF.

F. Valence response

Using the formal relation between the density matrix and the one-particle Green's function $\rho(E) = (-1/\pi)\mathrm{Im}\, G(E)$ one obtains from Eq. (21)

$$\rho^{\mathrm{val}}(\vec{r},\vec{r}',E) = \sum_{K,K'} R_{Kn}(\vec{r})\hat{\rho}_{Kn,K'n'}R_{K'n'}(\vec{r}'_{n'}), \tag{27}$$

which is valid for $\vec{r}$ in cell n and $\vec{r}'$ in cell n', where $R_{Kn}(\vec{r}) = \chi_K(\hat{r}_n)R_{\kappa n}(r_n)$. For real energies, the density matrix can be expressed entirely in terms of the regular solutions R_{Kn}, and the irregular solutions do not enter. Below the Fermi level on the real energy axis, the density matrix is a rapidly varying function of energy. Away from the real axis, however, the behavior is much smoother. To both retain the separable form of Eq. (27) and the smoothness obtained by calculating the Green's function away from the real axis, we introduce a small broadening Γ and renormalize the regular solutions, so that the central atom density matrix gives the same density of states (DOS) in each Norman sphere as the actual broadened density matrix:

$$\begin{aligned}
&\tilde{R}_{\kappa n}(r;E) = A_{\kappa n}(E,\Gamma)\,\mathrm{Re}\,\left[R_{\kappa n}(r;E+i\Gamma)\right],\\
&\int_0^{r_n^{\mathrm{Nrm}}}\left[\tilde{R}_{\kappa n}(r;E)\right]^2 r^2dr = \mathrm{Im}\int_0^{r_{\mathrm{Nrm}}} r^2dr\\
&\times\int_0^{r_n^{\mathrm{Nrm}}} r'^2dr' R_{\kappa n}(r_<;E+i\Gamma)H_{\kappa n}(r_>;E+i\Gamma).
\end{aligned} \tag{28}$$

This result is a key simplification in our approach. Here the Norman radius r_n^{Nrm} is defined as the radius of a neutral sphere centered on the n^{th} atom in the charge distribution formed by overlapping the charge distributions of the isolated atoms in their solid-state positions. The separable representation of the density matrix in Eq. (27) permits a separation of the double spatial integral in Eq. (16) into a product of two one-dimensional integrals. To complete the spatial integral in Eq. (16), we make the approximation that the spherical Norman cells n partition space and write the full integrals as sums of integrals over individual cells

$$\int d\vec{r} \longrightarrow \sum_n \int_{\vec{r}\in n} d\vec{r} = \sum_n \int_0^{r_N^{(n)}} r_n^2 dr_n \int d\Omega_n. \tag{29}$$

The dipole matrix elements at each site n are defined as

$$M^n_{K,K'}(E,E') = \int_{\vec{r}\in n} d\vec{r}\, \tilde{R}_{Kn}(\vec{r};E)\, d\, \tilde{\tilde{R}}_{Kn}(\vec{r};E')). \tag{30}$$

In the dipole approximation the matrix elements vanish except for transitions with $j' = j \pm 1$. Left (right) circularly polarized light only induces transitions with $m_j{}' = m_j + 1$ ($m_j{}' = m_j - 1$). Thus the transition matrix M is sparse. Relaxing the dipole approximation is straightforward. Doing so introduces additional non-zero elements to M. With these conventions, the contribution to the spectrum from the response of the valence states (i.e. those occupied single-particle states with eigenvalues above $E_{\rm cv}$) is given entirely in terms of density matrices and matrix elements,

$$\begin{aligned}\epsilon_2^{\rm val}(\omega) &= \frac{4\pi}{V}\int_{E_F-\omega}^{E_F} dE \sum_{n,n'} \mathrm{Tr}\, \rho_{nn'}(E) M_{n'}(E,E+\omega) \\ &\quad \times \rho_{n'n}(E+\omega) M_n^{\rm T}(E+\omega,E),\end{aligned} \tag{31}$$

where $\rho_{nn'}$ and M_n are matrices in a truncated relativistic angular momentum $K = (\kappa,\mu)$-space. By symmetry, the sum over sites n in Eq. (31) can be reduced to a sum over inequivalent sites in the solid. To compute $\epsilon_2^{\rm val}$ we first solve the Dirac equation at each inequivalent site which yields T. Then $G_{LnL'n'}$ is found by inverting the full multiple scattering matrix, and matrix elements M are evaluated using the wave functions from the calculation of T. Finally, Eq. (31) is evaluated using trapezoid rule integration for the energy integrals.

G. Spectrum construction

With the response of both the valence band and the more tightly bound electrons calculated, the contribution from each core edge is then interpolated onto a final output grid and combined with the other core edges and with the valence contribution:

$$\epsilon_2(\omega) = \sum_\nu \epsilon_2^{(\nu)}(\omega) + \epsilon_2^{\rm val}(\omega). \tag{32}$$

III. THEORETICAL OPTICAL CONSTANTS

The examples presented here are primarily monatomic crystals (metals and insulators) with a single inequivalent site. However, the generalization to heterogeneous materials is

straightforward, and an example is also presented for Al_2O_3. Non-periodic materials can be treated by including enough sites to converge the spectrum. The calculations presented in this section used FMS matrices truncated at $l = 3$ and 147 atoms for all materials except diamond. The diamond calculation used $l = 2$ and 450 atoms. We include Diamond because it is a difficult case for our real-space method even though typical k-space calculations of Diamond (such as the plane wave psuedopotential calculation shown in Fig. 5) use a unit cell containing only two atoms and can be less computationally demanding. All spectra were obtained by summing the contributions from 70 atoms. The response for the valence bands is obtained by calculating $\rho^{\rm val}$ on a regular energy grid of 200 points. Then the dipole matrix elements $M(E, E')$ are calculated for all pairs (E, E') with E below the Fermi level and E' above it. Eq. (31) is then evaluated by matrix multiplication and simple numerical integration. To compute $\epsilon_2^{\rm val}(\omega)$ to high frequencies, we employ an atomic model of the valence bands based on average band energies and occupations calculated from $\rho^{\rm val}$. The core state response is first calculated on a set of five 100 point frequency grids for each core initial state κ in the embedded-atom approximation. The FMS and path-expansion calculations are then carried out in cluster sizes of around 175 atoms on frequency grids of approximately 120 points. The contribution to ϵ_2 for each core initial state and the valence bands are then interpolated onto a large (5×10^5 points) frequency grid which spans the full spectrum (e.g. 10^{-3} through 10^6 eV) and serves as the final output grid. This grid has a higher density of points at low frequencies and around each core edge.

A. Dielectric function: Imaginary part

The fundamental quantity needed in our calculations of optical response is the imaginary part of the dielectric function $\epsilon_2(\omega)$ given by Eq. (32). All other optical constants can be obtained in terms of $\epsilon_2(\omega)$ as described below. As illustrative examples our density matrix calculations of $\epsilon_2(\omega)$ for Cu and Au are plotted in Fig. 1 compared to experiment. To demonstrate the effects of structural disorder on the dielectric response, we compare the imaginary part of the dielectric function for Diamond and amorphous Carbon in Fig. 32. Amorphous carbon structures were obtained with a "melt-and-quench" algorithm[32] using first principles molecular dynamics as implemented in the VASP package.[33] These results, as well as the results presented below and calculations for other materials, are currently

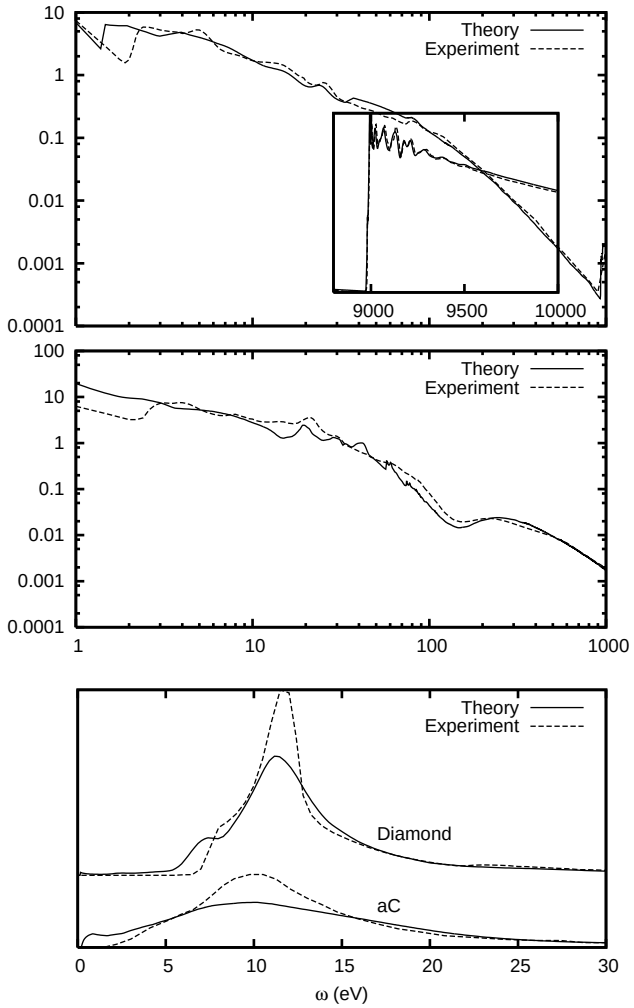

FIG. 1: Calculated and experimental ϵ_2 for Cu[29,30] (top), Au[29] (middle), and diamond[6] and amorphous C[31] (bottom). In the bottom panel the diamond curves have been shifted vertically for clarity.

available in both graphical and tabular form on the FEFF website.[34]

B. Dielectric function: Real part

Owing to the analyticity of the dielectric response, the real and imaginary parts of the dielectric function are related by the Kramers-Kronig relation[16]

$$\epsilon(\omega) = 1 + \frac{2}{\pi}\,\mathcal{P}\int_0^\infty d\omega'\frac{\omega'\epsilon_2(\omega')}{\omega^2-\omega'^2}. \tag{33}$$

Here $\mathcal{P}$ indicates the principal value of the integral. Since the denominator of the integrand in Eq. (33) has a pole at $\omega' = \omega$ care must be taken when evaluating the transform numerically.

To evaluate the integral appearing in Eq. (33) over the interval (ω_i, ω_{i+1}) between the i^{th} and $(i+1)^{\text{th}}$ grid points we find a linear approximation $\epsilon_2(\omega') = m\omega' + b$, which allows us to rewrite the Kramers-Kronig integral as follows:

$$\mathcal{P}\int_{\omega_i}^{\omega_{i+1}} d\omega' \frac{\omega'\epsilon_2(\omega')}{\omega^2 - \omega'^2} = m(\omega_{i+1} - \omega_i) + \frac{b - m\omega}{2}\ln\left(\frac{\omega_{i+1} + \omega}{\omega_i + \omega}\right) + \frac{b + m\omega}{2}\ln\left(\frac{\omega_{i+1} - \omega}{\omega_i - \omega}\right). \tag{34}$$

This expression is used to produce ϵ_1 on the same output grid used for the imaginary part. The results of this procedure for diamond, Cu and $Al_2O_3$are plotted in Fig. 2. Even though the numerical transform Eq. (35) is stable and accurate and (along with the calculated ϵ_2) completely determines ϵ_1 via Eq. (33), we find that the real part of the dielectric function is more sensitive to errors and approximations than the imaginary part.

C. Energy-loss

With both real and imaginary parts of $\epsilon(\omega)$ one can easily obtain the energy loss function

$$-\operatorname{Im}\epsilon^{-1}(\omega) = \frac{\epsilon_2(\omega)}{\epsilon_2^2(\omega) + \epsilon_1^2(\omega)}. \tag{35}$$

This is illustrated for Cu, Al_2O_3, and Au in Fig. 3. The loss function is proportional to the long-wavelength limit of the dynamic structure factor $S(\vec{q}, \omega)$, which can be measured by inelastic scattering of either electrons in electron energy loss spectroscopy (EELS) or photons in non-resonant inelastic x-ray scattering (NRIXS). Calculations of the latter performed in a framework similar to ours have recently been reported by Soininen et. al. who only address the response of core electrons, but at finite $\vec{q}$.[35] In contrast to ϵ_1 we find that the loss function is *less* sensitive to errors and approximations in the density matrix than ϵ_2. Onida, et. al[1]., in an illuminating discussion of the differences between absorption and EELS experiments, have given an explanation of this observation in terms of the long-range part of the coulomb interaction.

D. Index of refraction

The complex index of refraction is simply the square root of the complex dielectric function

$$n(\omega) + i\kappa(\omega) \equiv \epsilon(\omega)^{1/2}. \tag{36}$$

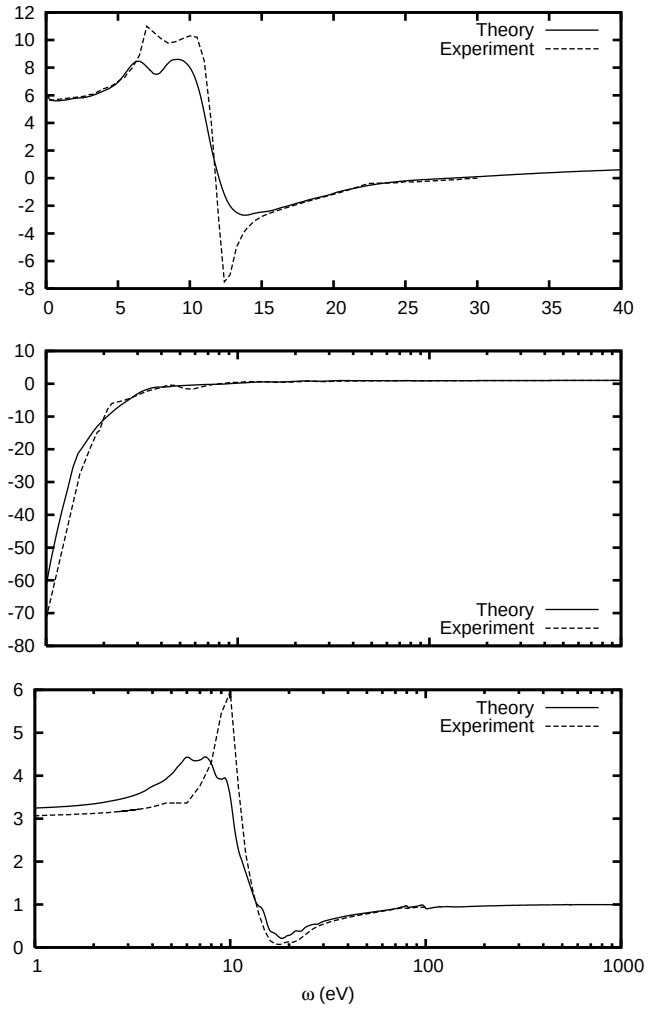

FIG. 2: Calculated ϵ_1 for diamond (top) and Cu (middle), and Al_2O_3(bottom) compared to experiment.[6,29]

Typical results for the real part of the index of refraction are given in Fig. 4.

E. Absorption coefficient

The photon absorption coefficient $\mu(\omega)$ is defined as the (natural) logarithm of the ratio of the incident and transmitted intensities for a photon beam across a thin sample, divided by the thickness. Theoretically $\mu(\omega)$ can be expressed in terms of the imaginary part of the index of refraction $\kappa(\omega)$

$$\mu(\omega) = 2\frac{\omega}{c}\kappa(\omega). \tag{37}$$

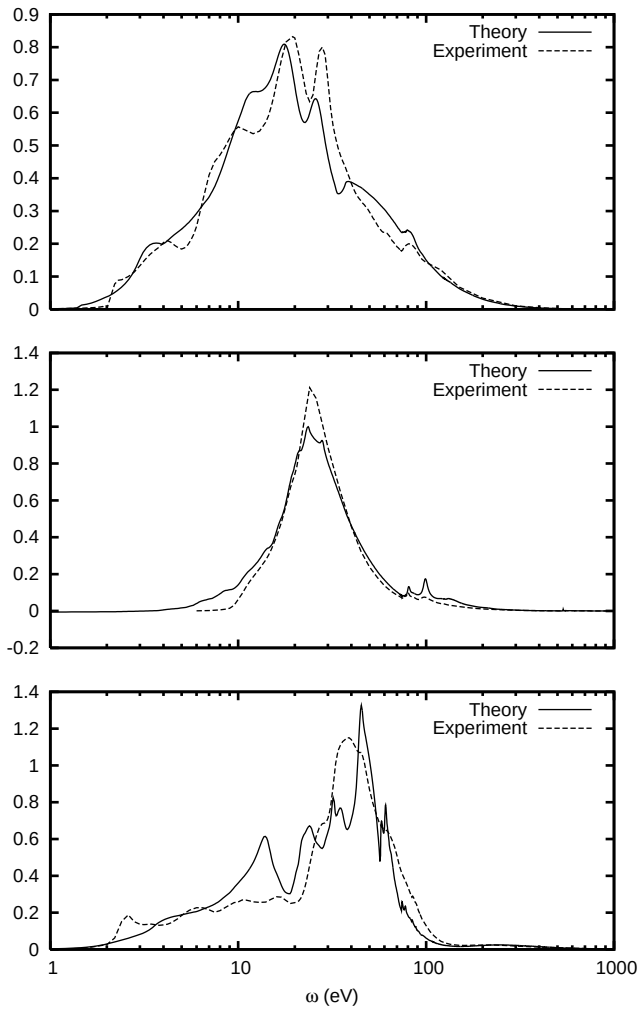

FIG. 3: Calculated energy-loss function (Eq. 35) for Cu (top), Al_2O_3(middle), and Au (bottom) compared to experiment.[6,29]

Thus, $\mu(\omega)$ is directly measurable with optical absorption experiments. Such experiments are currently performed to high accuracy using synchrotron light sources. We compare our calclulated results with experiment for several materials and with a calculation based on electronic structure calculated with ABINIT. This calculation was acomplished using the AI2NBSE package developed by Lawler, et. al.[36] which employs a BSE solver developed at NIST to generate optical spectra. The calculation shown excludes both local fields and excitonic effects and was generated using a regular grid of 8^3 k-points to sample the Brillouin zone, 50 bands, and an energy cutoff of 30 Hartree for the plane wave basis. The C 1_s electrons were treated with a Troullier-Martins psuedopotential. For a sensible comparision, no gap corrections were included in either calculation.

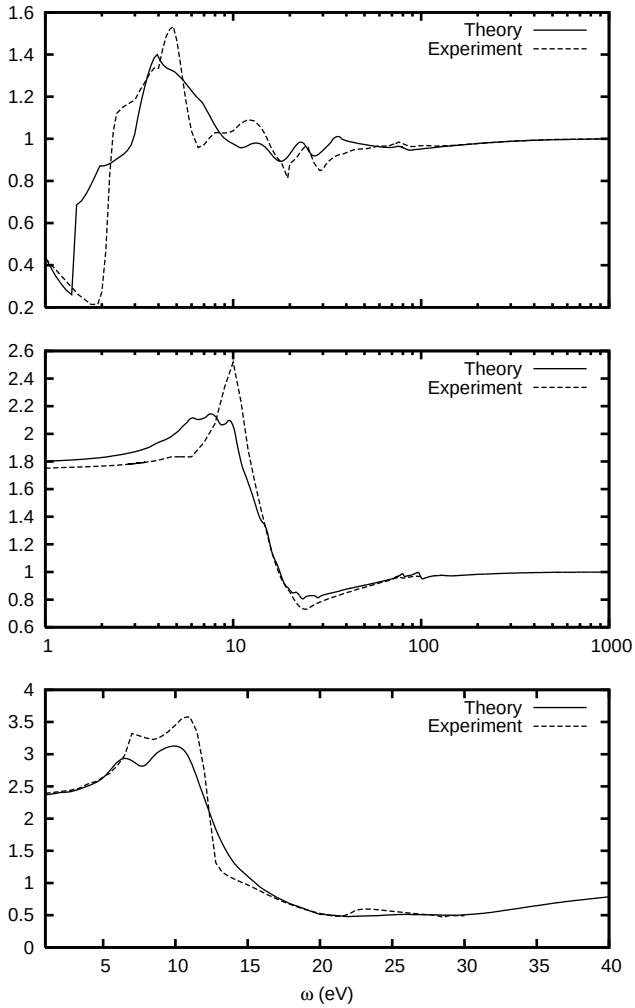

FIG. 4: Calculated real index of refraction for Cu (top), Al_2O_3(middle), and diamond (bottom) compared to experiment.[6,29]

F. Reflectivity

An important optical experiment for materials that can be prepared by vapor deposition methods is the measurement of the the reflectivity R defined as the ratio of the power reflected from a planar face of a sample to the incident power. This quantity can be related to the dielectric response of the material by considering the boundary conditions satisfied by Maxwell's equations at the interface between the sample and vacuum. This procedure produces the familiar Fresnel equations[16] relating the amplitudes of the transmitted (refracted) and reflected waves to the amplitude of the incident wave. As discussed by Stratton,[37] R

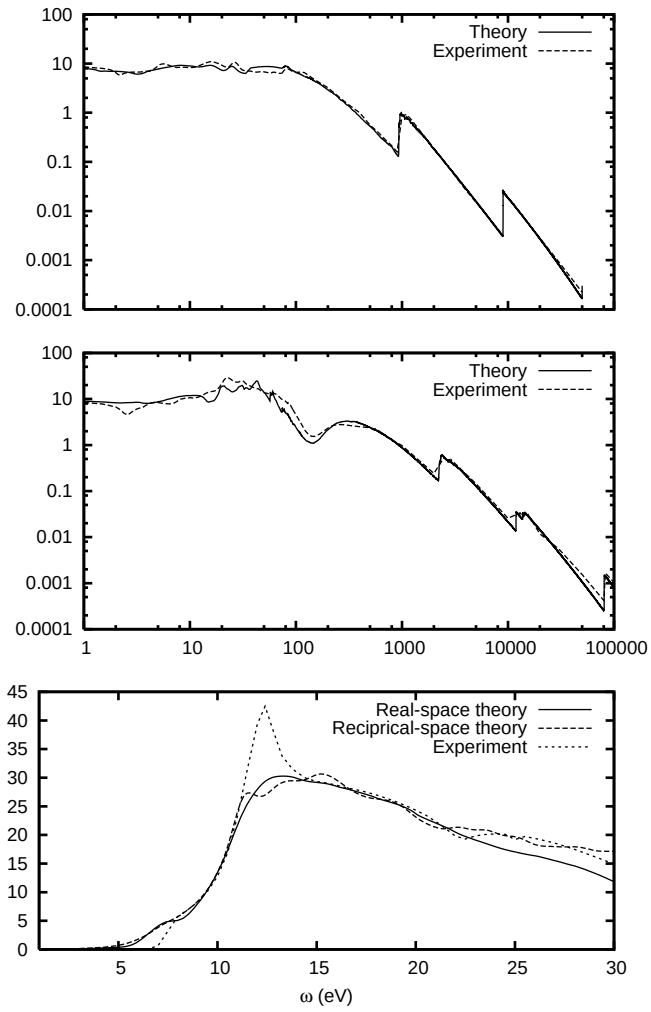

FIG. 5: Calculated absorption coefficient μ in inverse cm for Cu (top), Au (middle), and diamond (bottom) compared to experiment.[6,29] The calculated diamond result is also compared to a reciprocal-space calculation.

can be found by squaring the Fresnel equations. For example, for normal incidence

$$R(\omega) = \frac{[n(\omega) - 1]^2 + \kappa^2(\omega)}{[n(\omega) + 1]^2 + \kappa^2(\omega)}. \tag{38}$$

The general expression for a lossy material ($\epsilon_2 \neq 0$) and arbitrary angle of incidence is complex. However it is interesting to note that off normal incidence $R(\omega)$ has polarization dependence even for isotropic media.

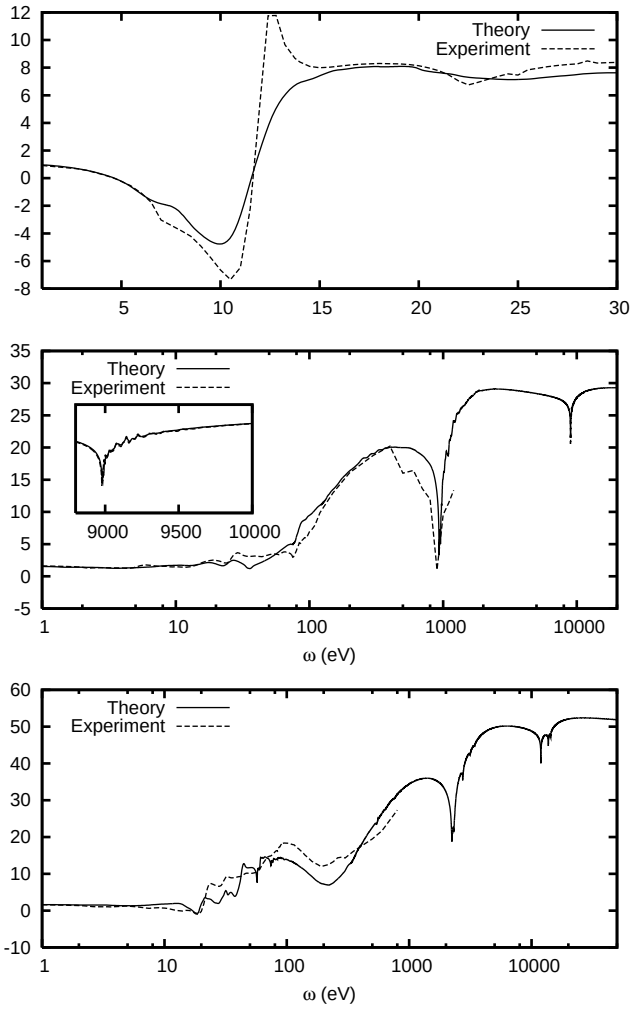

FIG. 6: Calculated real part of the anomalous atomic scattering factor for diamond (top), Cu (middle), and Au (bottom) compared to experiment.[6,29,39]

G. Photon scattering amplitude

The Rayleigh forward scattering amplitude $f(\omega)$ for photons can also be computed from the dielectric function[38]

$$f(\omega) = \frac{\omega}{4\pi r_0 c^2}\frac{V}{N}[\epsilon\,(\omega) - 1]\,. \tag{39}$$

Thus it is straightforward to calculate the x-ray scattering factors including anomalous terms using our RSMS approach $f(\vec{q},\omega) = g(q,\omega) + f^{ss}(\vec{q},\omega) + f_1(\omega) + if_2(\omega)$ in terms of f. Typical calculations of the real and imaginary parts of $f(\omega)$ are illustrated in Fig.'s 6 and 7.

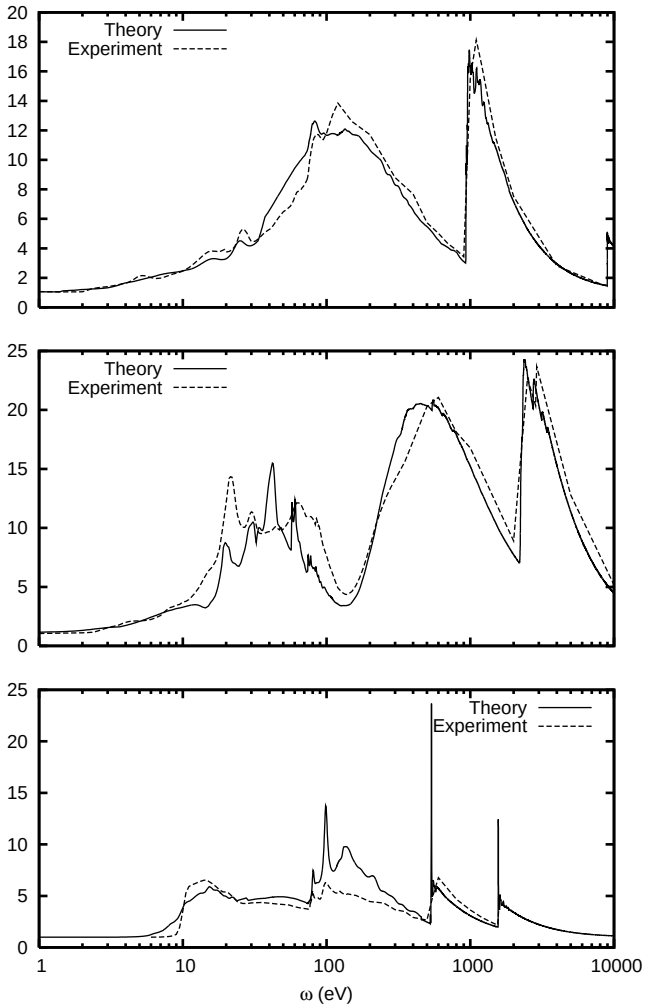

FIG. 7: Calculated imaginary part of the atomic scattering factor for Cu (top), Au (middle), and Al_2O_3(bottom) compared to experiment.[29]

IV. APPLICATIONS AND DIAGNOSITCS

A. Hamaker constant

The Hamaker constant is the (real) function $\epsilon(i\omega)$ of a real frequency ω. For separation distances beyond the tunneling regime, the interaction between the tip and sample in an atomic force microscopy experiment is dominated by the van der Waals force, which can be calculated given the tip-sample geometry and the Hamaker constants of the tip and sample.[40] Using the analyticity of ϵ in the upper half-plane, one can derive the following

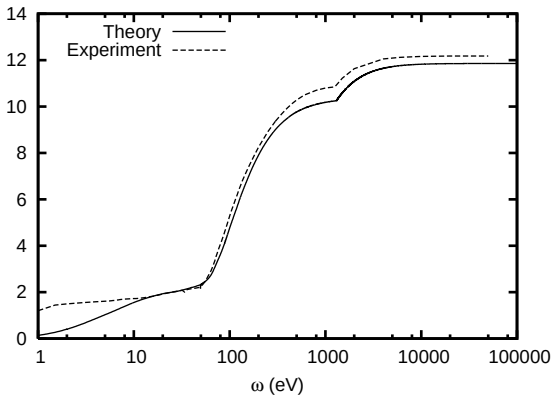

FIG. 8: $n_{\rm eff}(\omega)$ calculated from the ϵ_2 sum rule for Mg using Eq. (41), which assumes an asymptotic value of 12, the atomic number of Mg, in the $\omega \to \infty$ limit.

Kramers-Kronig type transform for the Hamaker constant

$$\epsilon(i\omega) = \frac{1}{\pi}\int_0^\infty d\omega\,' \frac{\omega\,'\epsilon_2(\omega\,') + \omega\epsilon_1(\omega\,')}{\omega^2 + \omega\,'^2}. \tag{40}$$

We evaluate Eq. (40) numerically in the same way we evaluate the Kramers-Kronig transform from ϵ_2 to ϵ_1, although away from $\omega = 0$ the integrand is regular.

B. Sum rules

Included in the output of our code are a few quantities useful for understanding the relationship between the underlying electronic structure and the frequency dependance of the optical constants. The f-sum rules for the imaginary parts of the dielectric function and the inverse dielectric function provide an important quantitative check of the calculation. We define the effective number of electrons per atom participating in transitions at frequency ω

$$n_{\rm eff}(\omega) = \frac{V}{2\pi^2 N}\int_0^\omega d\omega' \omega' \epsilon_2(\omega'). \tag{41}$$

This quantity has the limit[41]

$$\lim_{\omega\to\infty} n_{\rm eff}(\omega) = Z, \tag{42}$$

where Z is the number of electrons in the subsystem whose number density is N/V. The theory and calculations presented here are valid over a frequency range large enough to quantitatively evaluate the limit (42); missing or extra oscillator strength implies invalid

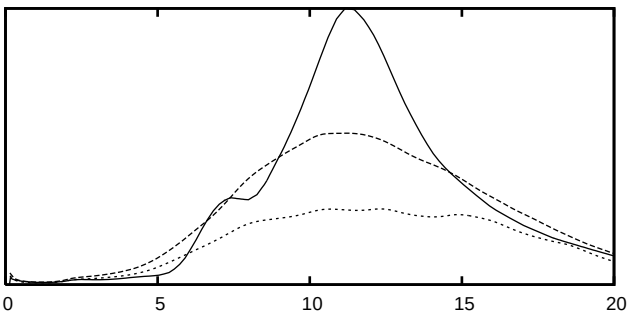

FIG. 9: JDOS/ω^2 for $p \to d$ (dashed line) and $p \to s$ (dots) transitions and the calculated ϵ_2 of this work (solid line) for diamond vs. photon frequency in eV.

approximations or unconverged calculations. Another check can be given by the index of refraction sumrule.

$$\int_0^\infty [n(\omega) - 1]\, d\omega = 0. \tag{43}$$

C. JDOS

As stated above, the selection rules constrain the angular momentum of final and initial states that can contribute to the absorption of light to a few channels (e.g. $p \to d$, $s \to p$, etc.). The joint density of states (JDOS) correspondig to a certain dipole allowed chanel ($l \to l'$) is defined in terms of the normal l-projected DOS ρ_l:

$$\int_{E_f-\omega}^{E_f} \rho_l(E)\rho_{l'}(E+\omega)\; dE, \tag{44}$$

where the l-projected DOS is given in terms of the density matrix by

$$\rho_l(E) = \sum_m \int d\vec{r}|Y_L(\hat{r})|^2 \rho(\vec{r},\vec{r},E). \tag{45}$$

Neglecting energy dependence of the dipole matrix elements in the calculation of ϵ_2 gives a spectrum which is a sum of terms proportional to the JDOS/ω^2 for the dipole allowed channels. We show this quantity for transitions from initial states with p character compared to the calculated ϵ_2 for Diamond in Fig. 9.

V. CONCLUSIONS

We have developed an efficient method for semi-quantitative *ab initio* calculations of optical constants over a broad spectrum, from the optical to x-ray frequencies. Our method, based on the one-particle density matrix, has been implemented in an extension of the RSGF approach in the FEFF codes which can be applied to general, aperiodic materials. We have illustrated the method here for a number of materials for which optical data are also available including metals, insulators and aperiodic solids. Overall our results for the optical constants are semi-quantitative in the optical-UV range, but become much more quantitative for x-ray energies. Also their imaginary parts tend to be more accurate compared to experiment. This degree of accuracy is already adequate for many purposes, and especially for models which are not particularly sensitive to the detailed fine-structure in the spectra such as the calculation of screened coulomb potentials and van der Waals interactions. Furthermore many improvements are possible: i) It is desirable to include local field corrections as described above; ii) the muffin-tin approximation should be replaced with more accurate *full potentials* in each cell; iii) the extension to arbitrary momentum transfer $\vec{q}$ is often desirable. As noted above, the calculations can be done for any momentum transfer with only a modest increase in computational effort within our density-matrix formulation. In fact, the response of core states has already been extended to finite q by Soininen, et. al;[35] iv) for crystalline systems, it may be desirable and sensible to calculate the MS matrix in k-space, i.e., with periodic boundary conditions; and v) the treatment of the particle-hole interaction K currently only takes intra-atomic screening into account.

Acknowledgments

We wish to thank A. Ankudinov, H. Lawler, G. Hug, E. Shirley, J. A. Soininen, A. Sorini, Y. Takimoto, and F. Vila for many helpful discussions. This work was supported in part by DOE Grant DE-FG03-97ER45623 and facilitated by the DOE CMSN.

---

[1] G. Onida, L. Reining, and A. Rubio, Rev. Mod. Phys. **74**, 601 (2002).

[2] P. Nozières and D. Pines, Phys. Rev. **109**, 741 (1958).

[3] H. Ehrenreich and M. H. Cohen, Phys. Rev. **115**, 786 (1959).

[4] S. L. Adler, Phys. Rev. **126**, 413 (1962).

[5] N. Wiser, Phys. Rev. **129**, 62 (1963).

[6] E. D. Palik, *Handbook of Optical Constants of Solids* (Academic Press, Orlando, 1985).

[7] W. T. Elam, B. D. Ravel, and J. R. Sieber, Rad. Phys. Chem. **63**, 121 (2002).

[8] B. L. Henke, E. M. Gullikson, and J. C. Davis, Atom. Data Nucl. Data Tables **54**, 181 (1993).

[9] J. J. Yeh and I. Lindau, Atomic Data and Nuclear Data Tables **32**, 1 (1985), URL `http://www.sciencedirect.com/science/article/B6WBB-4DBJ6HV-54/1/900634e5011c524427bd924083c`

[10] A. Zangwill and P. Soven, Phys. Rev. A **21**, 1561 (1980).

[11] E. Runge and E. K. U. Gross, Phys. Rev. Lett. **52**, 997 (1984).

[12] L. J. Sham and W. Kohn, Phys. Rev. **145**, 561 (1966).

[13] G. Strinati, Phys. Rev. B **29**, 5718 (1984).

[14] M. Rohlfing and S. G. Louie, Phys. Rev. B **62**, 4927 (2000).

[15] G. Rivas, Ph.D. thesis, University of Washington (2004).

[16] J. D. Jackson, *Classical Electrodynamics* (John Wiley & Sons, Inc., 1975).

[17] L. Reining, V. Olevano, A. Rubio, and G. Onida, Phys. Rev. Lett. **88**, 066404 (2002).

[18] I. Vasiliev, S. Öğüt, and J. R. Chelikowsky, Phys. Rev. Lett. **82**, 1919 (1999).

[19] A. V. Poiarkova and J. J. Rehr, Phys. Rev. B **59**, 948 (1999).

[20] I. P. Grant, Advan. Phys. **19**, 747 (1970).

[21] J. J. Rehr and R. C. Albers, Rev. Mod. Phys. **72**, 621 (2000).

[22] L. Hedin and S. Lundqvist, *Solid state physics: advances in research and applications* (Academic press, Inc., 1969), vol. 23, pp. 1–181.

[23] A. L. Ankudinov and J. J. Rehr, Phys. Rev. B **56**, R1712 (1997).

[24] A. L. Ankudinov and J. J. Rehr, Phys. Rev. B **62**, 002437 (2000).

[25] E. Tamura, Phys. Rev. B **45**, 3271 (1992).

[26] A. L. Ankudinov, B. Ravel, J. J. Rehr, and S. D. Conradson, Phys. Rev. B **58**, 7565 (1998).

[27] A. L. Ankudinov, S. I. Zabinsky, and J. J. Rehr, Comp. Phys. Comm. **98**, 359 (1996).

[28] S. I. Zabinsky, J. J. Rehr, A. Ankudinov, R. C. Albers, and M. J. Eller, Phys. Rev. B **52**, 2995 (1995).

[29] H. Hageman, W. Gudat, and C. Kunz, Tech. Rep., DESY (1974).

[30] M. Newville, Private comunication.

[31] S. Waidmann, M. Knupfer, J. Fink, B. Kleinsorge, and J. Robertson, Journal of Applied Physics **89**, 3783 (2001), URL http://link.aip.org/link/?JAP/89/3783/1.

[32] G. Galli, R. M. Martin, R. Car, and M. Parrinello, Phys. Rev. Lett. **62**, 555 (1989).

[33] G. Kresse and J. Furthmüller, Phys. Rev. B **54**, 11169 (1996).

[34] M. P. Prange, J. J. Rehr, and G. Rivas, *Full spectrum optical constants* (2007), URL http://leonardo.phys.washington.edu/feff/opcons/.

[35] J. A. Soininen, A. L. Ankudinov, and J. J. Rehr, Physical Review B (Condensed Matter and Materials Physics) **72**, 045136 (pages 10) (2005), URL http://link.aps.org/abstract/PRB/v72/e045136.

[36] H. M. Lawler, J. J. Rehr, F. Vila, S. D. Dalosto, E. L. Shirley, and Z. H. Levine, *Optical to uv spectra and birefringence of sio_2 and tio_2: First-principles calculations with excitonic effects* (2008), URL http://www.citebase.org/abstract?id=oai:arXiv.org:0807.1920.

[37] J. Stratton, *Electromagnetic Theory* (McGraw-Hill, 1941).

[38] A. L. Ankudinov and J. J. Rehr, Phys. Rev. B **62**, 2437 (2000).

[39] J. O. Cross, M. Newville, J. J. Rehr, L. B. Sorensen, C. E. Bouldin, G. Watson, T. Gouder, G. H. Lander, and M. I. Bell, Phys. Rev. B **58**, 11215 (1998).

[40] U. Hartmann, Phys. Rev. B **42**, 1541 (1990).

[41] M. Altarelli, D. L. Dexter, H. M. Nussenzveig, and D. Y. Smith, Phys. Rev. B **6**, 4502 (1972).

[42] J. J. Rehr and R. C. Albers, Phys. Rev. B **41**, 8139 (1990).

[43] J. S. Faulkner and G. M. Stocks, Phys. Rev. B **21**, 3222 (1980).

APPENDIX: REAL-SPACE MULTIPLE SCATTERING GREEN'S FUNCTION

In this Appendix we describe the real-space Green's functions used in this work. Formally the Greens functions operator is given by

$$G^+(E) = [E - H + i\delta]^{-1}, \tag{A.1}$$

where δ is a positive infinitesimal. Expanding G^+ in the scattering potentials and free propagators G^0 yields the multiple scattering (MS) expansion

$$\begin{aligned} G = G^0 + G^0 V G = \; & G^0 + G^0 T G^0 + \cdots \\ = \quad & [1 - \bar{G}^0 T]^{-1} G^0 \end{aligned} \tag{A.2}$$

Here we have introduced the local t-matrix $t_n = v_n + v_n G^0 t$ to sum implicitly over all scatterings at a given site n, where $\langle \vec{r}|t_n|\vec{r}'\rangle = t_n(\vec{r},\vec{r}',E)$ vanishes outside a given cell n where $v(r_n)$=0.

1. Free propagator

In position space the free propagator $G^0(E)$ is given by the FT,

$$G^0(\vec{r},\vec{r}',E) = \int \frac{d^3k}{(2\pi)^3} \frac{e^{i\vec{k}\cdot(\vec{r}-\vec{r}')}}{E - \frac{k^2}{2} + i\delta}. \tag{A.3}$$

Below we evaluate this expression in terms of site-angular momentum scattering states $|L,R\rangle$ which diagonalize t_i

$$\begin{aligned} j_L(\vec{r}_R) =& \langle \vec{r}|L,R\rangle = i^l j_l(kr_R) Y_L(\hat{r}_R) \\ \bar{j}_L(\vec{r}_R) =& \langle L,R|\vec{r}\rangle = i^{-l} j_l(kr_R) Y_L^*(\hat{r}_R), \end{aligned} \tag{A.4}$$

where $k = \sqrt{2(E-V_0)}$.

In terms of spherical Bessel functions the free propagator is given everywhere by

$$G^0(\vec{r},\vec{r}',E) = -2k \sum_L Y_L(\hat{r}) g_l(r,r') Y_L^*(\hat{r}') \tag{A.5}$$

$$= -2k \sum_L h_L^+(\vec{r}_>) \bar{j}_L(\vec{r}_<), \tag{A.6}$$

where $g_l(r,r') = h_l^+(kr_>) j_l(kr_<)$ and $h_L^+(\vec{r}) = i^l h_l^+(kr) Y_L(\hat{r})$. This result can be obtained, e.g., from the FT using the identity $\exp(i\vec{k}\cdot\vec{r}) = 4\pi\Sigma_L j_L(\vec{r}) Y_L^*(\hat{k})$ and carrying out the radial integrals in the complex k-plane. Alternatively the same result follows from the inhomogeneous radial differential equation, where the prefactor is obtained from the Wronskian $2/r^2 W(j_l, h_l^+) = -2k$. Here, as in the treatment of Rehr and Albers,[42] we have used the phase and normalization conventions of Messiah, with $j_l = (h_l^+ - h_l^-)/2i$ and $i^l h_l(x) = e^{ix} c_l(1/ix)/x$, c_l is a polynomial of degree l with $c_l(0) = 1$. Also, for convenience, we have included the phase factors i^l and i^{-l} in h_L^+ and $\bar{j}_L$ respectively, which do not change G^0, but simplify the asymptotic behavior.

The expansion of the free propagator for points at different sites has the form of a matrix

product

$$G^0(\vec{r},\vec{r}',E) = \sum_{L,L'} j_L(\vec{r}_R) G^0_{LR,L'R'} \bar{j}_L(\vec{r}_{R'}) \\ = \sum_{L,L'} \langle \vec{r}|LR\rangle \langle LR|G^0(E)|L'R'\rangle \langle L'R'|\vec{r}'\rangle. \tag{A.7}$$

This follows directly from Eq. (A.6) and the translation formulae for the spherical Hankel functions[42]

$$h^+_{L'}(\vec{r}'_R) = \sum_L j_L(\vec{r}_R)\, G^0_{LR,L'R'}. \tag{A.8}$$

Note the implicit factors of $i^{l'}$ and i^l in $j_L(\vec{r}_R)$ and $\bar{j}_{L'}(\vec{r}_R)$ in this representation. In some works, e.g. that of Faulkner and Stocks[43], these phase factors are included in the definition the propagator matrix elements. The above expression can be checked, e.g., by comparing $i^l h^+_l(kr) = \sum_{L'} j'_l(kr_R) i^{l'} G^{0+}_{L'R,L0}$. Eq. (A.7) can be derived, e.g., by expanding the exponential product $e^{i\vec{k}\cdot(\vec{r}-\vec{r}')} = e^{i\vec{k}\cdot(\vec{r}-\vec{R})} e^{-i\vec{k}\cdot(\vec{r}'-\vec{R}')} e^{i\vec{k}\cdot(\vec{R}-\vec{R}')}$ in spherical Bessel functions, and then carrying out the integration over k. This procedure yields for the dimensionless propagator matrix elements:

$$\tilde{G}^0_{LR,L'R'} \equiv \frac{G^0_{LR,L'R'}}{-2k} = 4\pi \sum_{L''} \langle Y_L Y_{L''}|Y_{L'}\rangle\, h^+_{L''}(k\vec{R}'').$$

which depend explicitly on $k\vec{R}'' = k(\vec{R}-\vec{R}')$. The FEFF code uses dimensionless matrix elements $\tilde{G}^0_{L,L'}(k\vec{R})$ which have a separable representation[42]

$$\tilde{G}^0_{L,L'}(k\vec{R}) \equiv \tilde{G}^0_{LR,L'R'} = \frac{e^{ikR}}{kR} \sum_\lambda \tilde{\Gamma}_{L\lambda} \Gamma_{\lambda,L'}, \tag{A.10}$$

$$\to 4\pi \frac{e^{ikR}}{kR} c_l c'_l Y^*_L(\hat{R}) Y_{L'}(\hat{R}),\ (kR\to\infty), \tag{A.11}$$

where $\Gamma_{\lambda,L}(k\vec{R})$ are generalized spherical harmonics. This can be obtained, for example, by substituting the asymptotic form of $i^l h_l$ and and the completeness relation $\sum_L Y^*_L(\hat{k}) Y_L(\hat{R}) = \delta(\hat{k}-\hat{R})$.

2. Full propagator

Let us now evaluate the behavior of the full propagator $G(\vec{r},\vec{r}',E)$ for $\vec{r}$ and $\vec{r}'$ in different cells n and n' respectively. For this case the MS series can be viewed as a sequence of

scattering events consisting of all scatterings at site n followed by all sequences of scatterings not scattering at site n first or site n' last, followed by all scatterings at site n',

$$G_{nn'} = [1 + G^0 t_n]\bar{G}_{nn'}[1 + t_{n'} G^0], \tag{A.12}$$

where the notation $G_{nn'}$ refers to the propagator starting and ending in cells n and n' respectively, while $\bar{G}_{nn'}$ refers to those terms in the MS expansion with first scatterings at sites other than n and last scatterings at sites other than n'. This can be evaluated by substituting the representation of Eq. (A.7) into Eq. (A.12) and then re-expressing the terms in the site-angular momentum basis. Then $\bar{G}_{nn'}$ can be expressed in terms of the dimensionless full multiple scattering matrix elements $\bar{G}_{Ln,L'n'}$ where

$$\begin{aligned} \bar{G}(\vec{r}, \vec{r}', E) &= \sum_{L,L'} j_L(\vec{r}_n)\, \bar{G}_{Ln,L'n'}\, \bar{j}_L(\vec{r}_{n'}) \\ \bar{G}_{Ln,L'n'} &= \left[1 - \bar{G}^0 T\right]^{-1} \bar{G}^0\big|_{Ln,L'n'} \end{aligned} \tag{A.13}$$

where $\bar{G}^0_{Ln,L'n'} = G^0_{Ln,L'n'}(1 - \delta_{nn'})$. The complementary delta-function in $\bar{G}^0$ ensures that $\bar{G}$ only includes initial scatterings from sites other than n and and final scatterings from sites other than n'. Next the terms on the left and the right sides of Eq. (A.12) can be expressed in terms of scattering states $R_{Ln}(\vec{r}_n)$. To see this note that matrix elements of the dimensionless t-matrices can be expressed in terms of phase shifts as

$$\begin{aligned} \langle j_L|\tilde{t}_n|j_{L'}\rangle &= \tilde{t}_{ln}\delta_{L,L'} \\ \tilde{t}_{ln} &= e^{i\delta_{ln}} \sin\delta_{ln}. \end{aligned} \tag{A.14}$$

Then using the representation of G^0 in terms of Bessel functions in Eq. (A.6), one obtains

$$\begin{aligned} \langle\vec{r}|[1 + \tilde{G}^0\tilde{t}_n]|LR\rangle &\equiv R_{Ln}(\vec{r}_n)e^{i\delta_{ln}} \\ &= i^l[j_l(r_n) + h_l^+(r_n)\tilde{t}_{ln}]Y_L(\hat{r}_n), (r_n > r_n^{\rm mt}), \end{aligned} \tag{A.15}$$

where $R_L(\vec{r}) = i^l R_{ln}(r)Y_L(\hat{r})$. Asymptotically $R_{ln}(r) = [h_l^+ e^{i\delta_{ln}} - h_l^- e^{-i\delta_{ln}}]/2i \to \sin(kr - l\pi/2 + \delta_{ln})/kr$. For $r < r^{\rm mt}$, the radial states can be obtained from the regular solution to the radial equation, matched to the above result. Similarly one obtains $\langle LR|(1+t_n G^0)|\vec{r}\rangle = \bar{R}_L(\vec{r}_n)\exp(i\delta_{ln})$. Note that the radial functions $R_{ln}(r)$ in the scattering states are real for real, nonnegative k, but are otherwise the analytic continuation to complex k. Combining

all these results in Eq. (A.12) then yields

$$\begin{aligned} & G(\vec{r},\vec{r}\,',E) = -2k \\ \times & \sum_{LL'} R_{Ln}(\vec{r}_n)\tilde{G}_{Ln,L'n'}\bar{R}_{L'n'}(\vec{r}_{n'}); \\ & \tilde{G}_{Ln,L'n'} = e^{i\delta_{ln}}\bar{G}_{Ln,L'n'}e^{i\delta_{l'n'}}. \end{aligned} \tag{A.16}$$

It is straightforward to show that this expression is equivalent to that of Faulkner and Stocks[43].

For $\vec{r}$ and $\vec{r}\,'$ at the same site n, $G = G^0 + G^0 t_n G^0 + \bar{G}_{n,n}$, where $\bar{G}$ is given by Eq. (A.13). This yields

$$\begin{aligned} G(\vec{r},\vec{r}\,',E) = -2k\Big[& \sum_{L} H_{Ln}(\vec{r}_>)\bar{R}_L(\vec{r}_<) \\ & + \sum_{L,L'} R_{Ln}(\vec{r}_n)\tilde{G}_{Ln,L'n}\bar{R}_{L'n}(\vec{r}_n)\Big], \end{aligned} \tag{A.17}$$

where $H_L(\vec{r})$ is the outgoing scattering state at site R which matches to $i^l e^{i\delta_{ln}} h_l^+(kr_n)$ for $r_n > r_n^{\rm mt}$.